Experimental Studies and Quantitative Modeling of Turing Patterns in the (Chlorine Dioxide, Iodine, Malonic Acid) Reaction

B. Rudovics, E. Barillot, P. W. Davies, E. Dulos, J. Boissonade,* and P. De Kepper*

Centre de Recherche Paul Pascal, CNRS Bordeaux, Avenue Schweitzer, F-33600 Pessac, France

Received: July 29, 1998; In Final Form: December 30, 1998

Experimental studies of the formation of Turing patterns in the (chlorine dioxide, iodine, malonic acid) reaction are performed in a spatial open gel disk reactor where all the input species are fed onto one side by a continuous stirred tank reactor. This setup is shown to fit the pool-chemical approximation used in most theoretical approaches. Nonequilibrium phase diagrams are established as a function of concentrations in the input flows. In agreement with theoretical predictions, the location of the transition from uniform steady states to Turing patterns is found to be almost independent of the concentrations of the complexing agent which controls the effective diffusion of activatory species. Extensive analytical and numerical calculations in two and three dimensions are performed on the basis of the Lengyel−Rábai−Epstein kinetic model and its two-variable reduction. This particular experimental configuration is shown to minimize the problems encountered with more commonly used versions of spatial open reactors. In standard conditions, the quantitative agreement with the experiments is excellent in regard to the sketchiness of the model. Finally, we discuss the role of boundary conditions and comment on problems they raise in the use of one-side-fed open spatial reactors.

1. Introduction

Far from thermodynamic equilibrium, organized concentration patterns can spontaneously develop in unstirred solutions of reacting and diffusing chemical species, as predicted by Turing in 1952.[1] Theoretical developments—often in a biological context—show that these stationary concentration patterns heavily rely both on competing activatory and inhibitory chemical mechanisms and on differences between the diffusion coefficients of species.[2−5] In particular, in two-variable systems, the activatory species must diffuse more slowly than the inhibitory species. The clear-cut experimental observation of a chemical Turing pattern was only achieved in late 1989,[6] on operating the chlorite−iodide−malonic acid (CIMA)[7,8] reaction in an open spatial reactor. This long awaited success triggered a renewal of experimental[9−11] and theoretical work on Turing structures (for an overview, see chapters 7−10 in ref 12).

Most of the theoretical and numerical works are based on formal chemical schemes.[13−20] However, some efforts to understand, at the chemical level, the mechanism of pattern formation observed with the CIMA reaction have been initiated by the Brandeis group.[21−27] The CIMA reaction is one among the very few reactions which can exhibit transient oscillatory dynamics when performed in batch conditions.[7] Lengyel, Rábai, and Epstein[28,29] have shown that when the reaction oscillates, most of the initial chlorite and iodide ions have been consumed and that the major species are then chlorine dioxide, iodine, and malonic acid. Appropriate mixtures of the three latter species exhibit oscillations immediately upon mixing and later also produced Turing patterns in an open spatial reactor.[24] These authors proposed a five-variable kinetic mechanism—hereafter referred as the Lengyel−Rábai−Epstein (or LRE) model—which accounts for the oscillatory behavior of batch mixtures of this CDIMA reaction.[28] They also derived a two-variable version of this mechanism. In this skeleton version, iodide and chlorite play respectively the role of the activator and of the inhibitor. Furthermore, to explain the observed Turing structures, Lengyel and Epstein suggested that the necessary slower diffusivity of the activator is obtained through a fast reversible immobilization on selective sites in the gel. The effective reduced diffusivity of iodide could be obtained by complexation of iodide by the macromolecules of starch initially used as color indicator or by the gel matrix itself.[21,22] This skeletonized mechanism is hereafter referred as the Lengyel−Epstein (or LE) model. Some of the predictions linked to the Lengyel and Epstein hypothesis were qualitatively confirmed by Agladze et al.,[31] who used the original CIMA reaction, and by Noszticzius et al.,[32] who used the CDIMA version of the reaction.

However, the experiments were performed in open spatial reactors made of a piece of gel where input species are fed by diffusion of two complementary subsets of chemicals from two opposite sides. In the most popular geometry presently in use, the reactor is made of a thin disk of gel fed onto the opposite faces.[10] This introduces parameter gradients in the direction orthogonal to the faces, leading to a continuous change of control parameters. In these conditions, a pattern, breaking the planar symmetry, eventually forms in regions where the values of these local parameters meet the conditions for a Turing instability, i.e., in a more or less thick stratum parallel to the disk faces.[23,33] There are several serious difficulties in modeling the formation of patterns in such devices. First of all, theory is much less developed for systems with gradients than it is for homogeneously fed systems. Second, the input species concentrations are only fixed on the boundaries and their gradients inside the gel are actually unknown. Finally, the structures are intrinsically three-dimensional. In this respect, in the gel disk reactor, the patterns are observed in a direction orthogonal to the faces, so that the light absorption is averaged over the film thickness. If the structured stratum is thicker than one wavelength, the determination of the 3-D pattern geometry is not straightforward and specific arrangements must be used.[34,35] When the structure is confined within a monolayer by the gradient, it was shown

10.1021/jp983210v CCC: $18.00
Published on Web 03/06/1999

that the patterns are similar to those of a genuine 2-D system but that their stability and their selection can be significantly modified.[36] This makes difficult a quantitative comparison between the model predictions and the experimental observations. Note that Lengyel and Epstein observed transient Turing patterns and waves in a gradient-free unstirred batch solution of the CDIMA reaction in the presence of starch.[26] However, because of unavoidable parameter drifts, and critical slowing down phenomena, a clear determination of the bifurcation values are generally not possible in closed systems.

In this paper, we present a systematic study of Turing patterns and dynamical instabilities in a gradient-free reaction−diffusion system which could be easily modeled. The main objective was to check quantitatively the assumptions and predictions of the LE model, especially concerning the effects of the complexing agents on the Hopf and Turing bifurcations. In order to get experiments and theory in closer connection, we used an open reactor that overcomes most of the above mentioned difficulties. According to the work of Lengyel and Epstein, in the CDIMA reaction, if no external gradients are imposed, the variations of the input species concentrations are small on the distance of a wavelength or over a period of oscillation. If all the input reactants are fed onto one side of a thin enough film of gel—i.e. the thickness is about one wavelength or less—we expect the concentrations of these reactants to be almost constant in space and time all through the gel. Accordingly, the film should be a good approximation of a 2-D system with homogeneous constraints. The price to pay is that reaction already proceeds in the reservoir. In order to exert a control on the boundary conditions, this reservoir must be a continuous stirred tank reactor (CSTR) with well-defined input flows. Then, the actual concentrations onto the feed-face are not those of the input flows but result from the system dynamics. We shall see that this can be easily taken into account.

In the spirit of an approach which has proved its efficiency in the study of oscillating reactions, we have used this setup to establish the topology of nonequilibrium phase diagrams.[38] These experimental diagrams and various properties of the system will be analyzed together with those obtained by numerical simulations of the LE model of the reaction.

In section 2, we first describe the reactor and provide a brief review of the reaction used in this work. We subsequently present the LRE and the LE models of the reaction, our modeling strategy, and the analytical and numerical techniques.

In section 3, we report in parallel the experimental observations and the numerical predictions. In section 3.1, we establish the phase diagram for the homogeneous reaction in a CSTR. These and other results are used to assign appropriate values to kinetic constants that were previously fixed more or less arbitrarily in the literature.

In section 3.2—the core of the paper—we present an extensive study of the phase diagrams in the 2-D limit and discuss the role of the various parameters, in particular the role of the concentration of the complexing agent.

In section 4, we summarize and discuss the results and draw conclusions. More precisely, we point out the limits of the different approximations and discuss the effects of the genuine boundary conditions when the two-dimensional hypothesis is dropped. The specific role of the interfacial region that links the CSTR and the gel film is underlined.

2. Experimental and Modeling Techniques

2.1. Experimental Setup. Different geometries of open spatial gel reactors have been developed to study sustained chemical patterns. In such devices, soft hydrogels are used as reaction media to prevent the reacting solutions from convection. In these hydrogels, small solvated molecules and ions diffuse practically as in plain water.

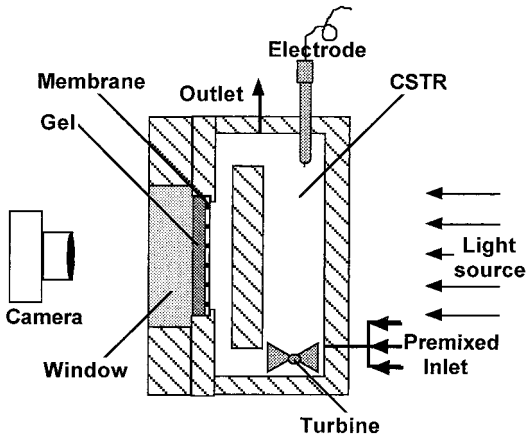

Figure 1. One-side-fed gel disk reactor. Schematic representation of a transversal section. Chemical patterns develop in the disk of gel. The CSTR controls the feed composition imposed on one side of the disk.

A schematic representation of the reactor is given in Figure 1. It consists of a continuous stirred tank reactor (CSTR) and a very thin transparent disk of agarose gel (0.2 mm thick, 20 mm diameter), one face of which is in contact with the contents of the CSTR. The opposite face is pressed against a planar, impermeable, solid back. Between the disk of gel and the CSTR, an inorganic membrane (Anotec from Whatman with unidirectional pore size 0.02 μm) rigidly maintains the gel. To reinforce the membrane and improve its adhesion with the disk of gel it is impregnated with a 8% agarose gel. Its main role is to cut down the hydrodynamic turbulence which could distort the patterns developing inside the disk. Moreover, it introduces a decoupling factor between the dynamics of the CSTR and that of this gel disk. This point will be discussed in section 4. The disk is obtained by cooling in a shape a hot solution of 2% agarose (Fluka 05070) containing well-defined concentrations of poly(vinyl alcohol) (Sigma MW 9000). Poly(vinyl alcohol) (PVA) acts both as a color indicator of polyiodide ions and as a complexing agent governing the effective diffusivity of complexed ions in particular the diffusivity of I^-, a species controlling the activatory process in the CDIMA reaction.

The unusual toroidal shape of the CSTR was designed to minimize the thickness of the colored fluid layer through which the observations of the gel are made and to produce a rapid uniform renewal of the reacting solution immediately in contact with the inorganic membrane. This renewal is obtained by a turbine which produces fast mixing and recirculation with a characteristic time less than 2 s.

The CSTR is continuously refreshed by constant flows of chlorine dioxide, iodine, and malonic acid. These chemical solutions are set in three separated vessels, all containing 1.0×10^{-2} M sulfuric acid. The malonic acid solution also contains a controlled concentration of PVA in order to avoid long term losses of PVA from the disk and to keep the CSTR in an appropriate stationary state. All chemicals, of analytical purity, are used without further purification. Stock solutions of chlorine dioxide are prepared from the reaction of sodium chlorite with sodium peroxodisulfate in strongly acidic solutions. The gaseous ClO_2 thus formed is carried away, with a stream of air, and redisolved in a flask containing ice-cold distilled water.[39] The concentrations of the stock solutions of ClO_2, stored in the dark at 4 °C, are checked every 2 days by iodometric titration. Equal

flows coming from the three vessels are injected premixed by precision piston pumps into the CSTR through a three-way inlet port. The residence time of the CSTR is $\tau = 480$ s. All experiments were performed at a temperature of 4.5 °C ± 0.5 °C with a fixed iodine feed concentration $[I_2]_0 = 3.0 \times 10^{-4}$ M.

A bright platinum electrode measures the redox potential in the CSTR and provides a qualitative characterization of states. The evolution of the patterns in the gel is monitored by a black and white CCD camera linked to a contrast-enhancing device (Hamamatsu C2400). The images, stored on a VCR, are further analyzed by image processing.

In the experimental section, the concentrations of the input species, bracketed in the text by $[\,]_0$, correspond to the concentrations that these reactants would have after mixing in the total inlet flow and prior to any reaction. The concentrations of the volatile species, chlorine dioxide and iodine, in the input flows are corrected for the losses by diffusion through the Teflon injection tubings.

2.2. Kinetic Models. On the basis of various kinetic studies of separated subsets of reactions,[40,42,43] Lengyel, Rábai, and Eptein have shown that the main dynamical features of the CDIMA reaction could be accounted by the following set of stoichiometric equations:[28,29]

$$\begin{aligned} MA + I_2 &\rightarrow IMA + I^- + H^+ \\ ClO_2 + I^- &\rightarrow ClO_2^- + {}^1/_2 I_2 \\ ClO_2^- + 4I^- + 4H^+ &\rightarrow 2I_2 + Cl^- + 2H_2O \end{aligned} \qquad (1)$$

Here MA, I_2, ClO_2, ClO_2^-, and I^- are the independent variables, $[H^+]$ is considered as constant, and Cl^- and IMA are inert products. To account for the fast reversible complexation of I^- and I_2, the following mass balance equation is introduced:

$$S + I_2 + I^- \rightleftharpoons SI_3^- \qquad (2)$$

Here S represents the complexing sites for I^-—in our experiments these sites are provided by the poly(vinyl alcohol)—and SI_3^- is a symbolic species that holds for a series of different polyiodide complexes in fast equilibrium. As in ref 30, the rate equations for eqs 1 and 2 are

$$\begin{aligned} r_1 &= \frac{k_{1a}[MA][I_2]}{k_{1b} + [I_2]} \\ r_2 &= k_2[ClO_2][I^-] \\ r_3 &= k_{3a}[ClO_2^-][I^-][H^+] + \frac{k_{3b}[ClO_2^-][I_2][I^-]}{\alpha + [I^-]^2} \\ r_4 &= k_4[S][I_2][I^-] - k_{-4}[SI_3^-] \end{aligned} \qquad (3)$$

In the absence of external feed and convection, the concentration changes are ruled by the system of equations

$$\begin{aligned} \frac{d[MA]}{dt} &= -r_1 + D_{MA}\Delta_{\mathbf{r}}[MA] \\ \frac{d[I_2]}{dt} &= -r_1 + {}^1/_2 r_2 + 2r_3 - r_4 + D_{I_2}\Delta_{\mathbf{r}}[I_2] \\ \frac{d[ClO_2]}{dt} &= -r_2 + D_{ClO_2}\Delta_{\mathbf{r}}[ClO_2] \\ \frac{d[S]}{dt} &= -r_4 \\ \frac{d[I^-]}{dt} &= r_1 - r_2 - 4r_3 - r_4 + D_{I^-}\Delta_{\mathbf{r}}[I^-] \\ \frac{d[ClO_2^-]}{dt} &= r_2 - r_3 + D_{ClO_2^-}\Delta_{\mathbf{r}}[ClO_2^-] \\ \frac{d[SI_3^-]}{dt} &= r_4 \end{aligned} \qquad (4)$$

where the molecular diffusion terms have been introduced. Since the complexing agent and the complex are large macromolecules, their diffusion in the gel is negligible and the respective diffusion terms have been dropped out. The following constants are set to the values found in the literature and adjusted at 4 °C by Lengyel and Eptein:[21,22,27−29,44] $k_{1a} = 6.2 \times 10^{-4}$ s^{-1}, $k_{1b} = 5 \times 10^{-5}$ M, $k_2 = 900$ M^{-1} s^{-1}, $k_{3a} = 100$ M^{-2} s^{-2}, $k_{3b} = 9.2 \times 10^{-5}$ s^{-1}, $D_{MA} = 0.4 \times 10^{-5}$ cm^2 s^{-1}, $D_{I_2} = 0.6 \times 10^{-5}$ cm^2 s^{-1}, $D_{ClO_2} = 0.75 \times 10^{-5}$ cm^2 s^{-1}, $D_{I^-} = 0.7 \times 10^{-5}$ cm^2 s^{-1}, $D_{ClO_2^-} = 0.75 \times 10^{-5}$ cm^2 s^{-1}. The values we used for k_4, k_{-4}, and α will be discussed later.

When the reaction is performed in a CSTR, the diffusion terms must be replaced by flow terms of the form $k_E([X]_0 - [X])$, where $[X]$ is the concentration of species X in the reactor and k_E is the inverse of the residence time. In the following, k_E will be fixed at the value $k_E = 2 \times 10^{-3}$ s^{-1}.

In agreement with experimental observations, $[I^-]$ and $[ClO_2^-]$ undergo much larger changes in time and space than the concentrations of the input species. Lengyel and Epstein have shown that, under these conditions, system (4) can be reduced to a system of two normalized kinetic equations[22,27,44]

$$\begin{aligned} \frac{\partial u}{\partial \tau} &= \frac{1}{\sigma}\left(a - u - 4\frac{uv}{1+u^2} + \Delta_{\mathbf{r}'}u\right) \\ \frac{\partial v}{\partial \tau} &= b\left(u - \frac{uv}{1+u^2}\right) + d\Delta_{\mathbf{r}'}v \end{aligned} \qquad (5)$$

with

$$\begin{aligned} u &= \frac{[I^-]}{\sqrt{\alpha}} \quad v = \left(\frac{k_{3b}[I_2]}{\alpha k_2[ClO_2]}\right)[ClO_2^-] \quad d = D_{ClO_2^-}/D_{I^-} \\ a &= \left(\frac{k_{1a}[MA]}{\sqrt{\alpha}k_2[ClO_2]}\right)\left(\frac{[I_2]}{k_{1b} + [I_2]}\right) \quad b = \frac{k_{3b}[I_2]}{\sqrt{\alpha}k_2[ClO_2]} \\ \sigma &= 1 + \frac{k_4}{k_{-4}}[S]_0[I_2] \quad \tau = k_2[ClO_2]t \quad \mathbf{r}' = \left(\frac{k_2[ClO_2]}{D_{I^-}}\right)^{1/2}\mathbf{r} \end{aligned} \qquad (6)$$

where τ and $\mathbf{r}'$ respectively rescale the time and space units. Systems (4) and (5) are what we refer as the LRE and LE models. Before we proceed further, a few points that are often overlooked deserve special comments.

Parameter α is a somewhat ad hoc constant. Experimental studies[40,42] predict that the second term in rate law r_3 (see eq 3) is of the form $k_{3b}[ClO_2^-][I_2]/[I^-]$ over a large range of concentrations. However, the validity of this simple rate law cannot hold for very low $[I^-]$ since it gives $r_3 \rightarrow \infty$ when $[I^-] \rightarrow 0$ whereas one obviously expects $r_3 \rightarrow 0$. Several authors[29,45] have introduced the constant α and replaced the original term $1/[I^-]$ given by Kern and Kim[40] by $[I^-]/(\alpha + [I^-]^2)$ in order to restore coherence at this level. One can consider $\sqrt{\alpha}$ as a cutoff concentration for $[I^-]$. Above this cutoff, the modified rate law fits well the experimental data within the considered range, but below this value, the inhibitory character of term r_3 drops out as expected. This cutoff was generally fixed at low reasonable but arbitrary values ($\alpha \sim 10^{-12}-10^{-14}$). Although these small changes could appear as a minor point, it occurs that all essential quantities related to Turing patterns, such as the critical values, the pattern amplitudes, etc., depend explicitly on α. Actually, the switch between inhibitory and noninhibitory regimes is one of the sources for the Turing pattern formation. These properties impose severe restrictions in the use of the LE model. First, the constant α should not be chosen arbitrarily but in direct connection with experimental results. Second, the rate law r_3 should not be used for $[I^-] \ll \sqrt{\alpha}$. Beyond this limit, the kinetic law should no longer be parametrized by introducing a simple constant term. As a result, it is not possible to describe quantitatively the formation of the patterns in systems where concentration gradients of input species lead to vanishing $[I^-]$ in some regions of the system, as it is the case in the original experiments with the CIMA reaction. Attempts to account for this category of experiments should require a more involved description of the kinetics that could possibly be derived from the very detailed mechanism recently proposed by Lengyel et al.[41] The alternative is to perform the experiments in the absence of strong gradients, keeping the input species concentrations in a domain where the model is valid. We shall see that the use of a one-side-fed reactor precisely meets these requirements and allows for an appropriate use of the simple LE model.

In the absence of precise data on the actual concentration of complexing sites per mass unit of polymer, we have arbitrarily set k_{-4} to unity, a value already chosen by Lengyel and Epstein and we have estimated that a concentration of complexing agent $[S] = 10^{-3}$ corresponds to 1 g/L of PVA; the constants $K = k_4/k_{-4}$ and α were simultaneously adjusted to the values $\alpha = 10^{-15}$ and $K = 10^8$ (i.e. $k_4 = 10^8$) in order to fit at best a few selected experimental transition points (e.g. onset of oscillations or of Turing patterns) and oscillation periods.

2.3. LE Model: Theoretical Predictions. Although the LE model has become very popular, only a few analytical properties of this model are presently available in the literature. We have derived some important analytical results that were completed by 2-D numerical simulations to understand the basic dynamical properties of this model.

Close to onset, Hopf bifurcations, Turing bifurcations, and pattern selection are generally studied in terms of amplitude equations[15,46] that can be derived by multiple time and length scales analysis.[50] Starting from these equations, commonly used in nonlinear dynamics, one can determine the selection of standard patterns close to onset[51,52] as it was done for the Brussellator[18] or other models leading to Turing structures.[36] In a two-dimensional space, these are hexagon and stripe patterns. The amplitude equations for the LE model have been derived for 2-D systems with constant and uniform parameters by several authors.[37,53] Here, we only report the results (as explicitly expressed in ref 53) that are essential to understand the next steps. They can be obtained from the linear stability analysis and from the complicated expressions of the coefficients of the nonlinear amplitude equations. The ratio $d = D_{ClO_2^-}/D_{I^-}$ is a fixed quantity. When parameter d was involved, we used the experimental value $d = 1.07$ reported in ref 27. The complexing agent is involved only through parameter σ. Acceptable experimental values are within the range $1 \leq \sigma < 1000$. We used b as the bifurcation parameter. The results are gathered in diagrams drawn in the plane (a,b) and represented in Figures 2 and 3.

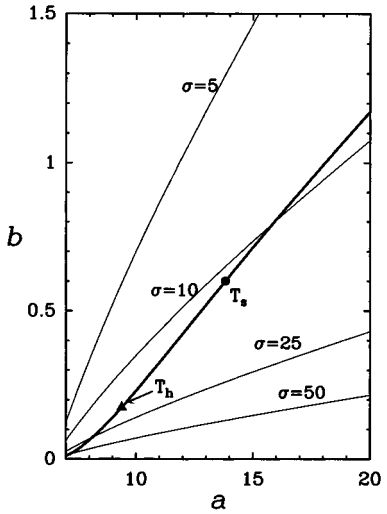

Figure 2. Bifurcations of the Lengyel−Epstein model. Key: **−** Turing bifurcation; —, Hopf bifurcation at various values of σ. At T_h, H_0 hexagon patterns change to H_π; at T_s, stripe patterns become subcritical.

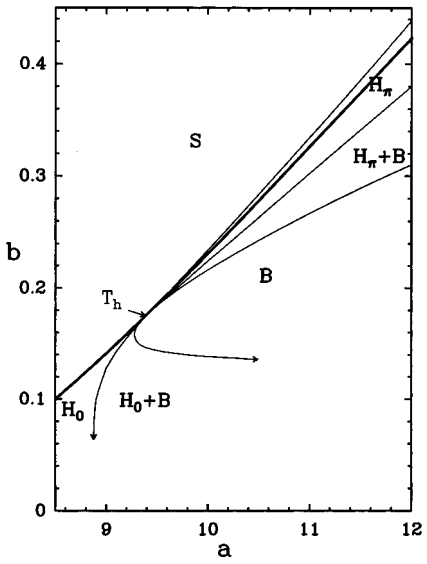

Figure 3. Pattern selection in the Lengyel−Epstein model. Key: **−**, Turing bifurcation; —, limits of stability of the different patterns. S: uniform stationary pattern. H_0: H_0 hexagon patterns. H_π: H_π hexagon patterns. B: stripe patterns.

In Figure 2, we show the lines where the homogeneous stationary state loses stability. The full line represents the locus of the bifurcation to a Turing structure given by

$$b_T = \frac{d}{5a}(13a^2 - 4\sqrt{10}a\sqrt{25 + a^2} + 125) \qquad (7)$$

with the wavelength

$$\lambda_c = 2\pi\sqrt{\frac{\sqrt{25+a^2}}{2\sqrt{10}a - 5\sqrt{25+a^2}}} \tag{8}$$

The bifurcation point b_T and the wavelength λ_c are independent of σ. Initially shown by Lengyel and Epstein,[22] this property is in agreement with the extended theory of Pearson and Bruno.[47] These authors predict that, when the diffusion is controlled by formation of a non reactive immobilized complex, the Turing bifurcation point does not depend on the concentration [S] of the complexing agent because, in this case, σ simultaneously renormalizes the reactive term and the diffusion term. Thin curves show the Hopf bifurcation for different values of σ. The instability occurs at

$$b_H = \frac{3a^2 - 125}{5a\sigma} \tag{9}$$

with the period

$$T_c = 2\pi\sigma\sqrt{\frac{25+a^2}{5(3a^2-125)}} \tag{10}$$

Note that Turing and Hopf bifurcations both occur when b decreases. Thus, at low values of [S], precisely for $\sigma < (26 + 8\sqrt{10})/6d \simeq 7.99$, the Hopf bifurcation always precedes the Turing bifurcation so that the system becomes oscillatory first. Above this value, the Turing bifurcation occurs first within an interval of parameter a which rapidly increases with σ (accordingly with [S]) and a stationary spatial pattern can form.

Additional information on pattern selection can be obtained from the signs of the coefficients of the amplitude equations. In the standard selection scheme[15,17,18,51,52] a stable hexagonal pattern bifurcates first subcritically. A stripe pattern bifurcates supercritically but is unstable. When the distance to the bifurcation point increases, the stripe pattern gains stability, before the hexagonal pattern becomes unstable in turn. Thus the natural sequence is homogeneous−bistable (uniform/hexagons)−hexagons−bistable (hexagons/stripes)−stripes. The extent of the subcritical region overwhich the hexagonal pattern and the homogeneous steady state are simultaneously stable is related to a second-order term and is usually very small. There are two types of hexagons, referred to as H_0 and H_π, respectively when the maxima (Figure 4a) or the minima (Figure 4c) of amplitude form the hexagonal network. The nature of the hexagons at the transition is determined by the sign of the quadratic term in the amplitude equations. For the LE model, a change of sign occurs at point T_h on Figure 2, at $a = a_h = 5[(6 + \sqrt{21})/3]^{1/2} \simeq 9.3908$. Hexagons H_0 are obtained when $a < a_h$, and hexagons H_π, when $a > a_h$. At point T_h, the domain of hexagons vanishes and the stripes are stable right away. Another remarkable point is point T_s (where $a = a_s \simeq 13.8254$). When $a > a_s$, all patterns (hexagons and stripes) become subcritical so that the subcritical domain can become quite large. In this region where localization phenomena are possible,[55] the concentration changes become very stiff. They form steep fronts that are almost frozen in time so that the patterns would not reorganize on realistic experimental times. Computed examples of the different patterns are presented in Figure 4. We have established, by numerical simulation, the effective stability of the different types of patterns with wavelength λ_c in the vicinity of point T_h. The results are gathered in Figure 3. Note that, far from the transition, the sideband of unstable wavelength increases rapidly so that the selection of patterns with $\lambda \neq \lambda_c$ should be considered. Moreover, for a point far from the bifurcation, the value λ_c to be used in the numerical tests differs with the choice of the bifurcation parameter (e.g. a at constant b or b at constant a), so that the stability of the different patterns cannot be determined unambiguously. To indicate that a stability limit is no longer significant in this respect, it is terminated by an arrow in the diagram. Note the existence of reentrant hexagons[18,36] when $|b - b_T|$ increases.

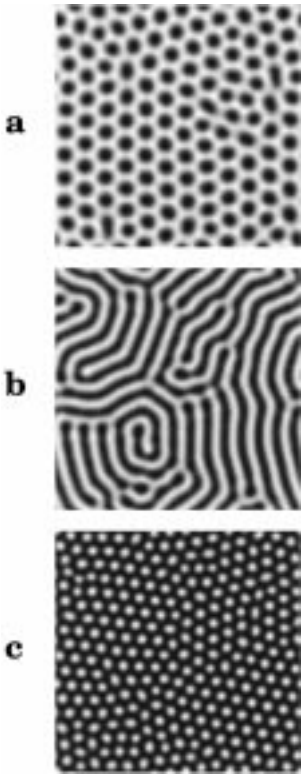

Figure 4. Typical Turing patterns in the Lengyel−Epstein model ($\sigma = 50$): (a) H_0 pattern, $a = 8.8$, $b = 0.09$; (b) stripe pattern, $a = 10$, $b = 0.16$; (c) H_π pattern, $a = 12$, $b = 0.39$.

2.4. Computational Methods. In a preliminary stage, we have checked the basic hypothesis on which our experimental and numerical approaches rely. To do so, we have first studied the CSTR coupled with a linear one-dimensional reactor of length l, where $l = 0.2$ mm corresponds the thickness of the gel with the seven-variable LRE model (eqs 4). The ratio of the CSTR volume V to the gel volume v is involved in the exchange rate between the CSTR and the gel. It was fixed to the typical experimental value $V/v = 200$. The equations were integrated numerically by finite differences (coupled cells) with a fourth-order Rosenbrock time integrator.[48] The first cell corresponds to the CSTR, taking into account the possible feedback on the CSTR dynamics. The first cell inside the 1-D reactor is diffusively coupled to the CSTR cell. No-flux boundary conditions are used on the opposite side. In this configuration, we investigated the effect of the gel depth, in particular on the profile of the input species concentrations, to check the homogeneity of these input species, and we computed their concentrations within the CSTR, as a function of the concentrations in the input flow. These computed values are precisely those which have to be maintained at the CSTR−gel interface. Note that, due to the large value of V/v, one finds that the reactions in the gel have practically no influence on the CSTR dynamics. On the contrary, if the CSTR contents enters into an oscillatory state, it normally forces oscillations in the gel. Two typical examples of the concentration profiles of all species, in a regime for which computed Turing patterns

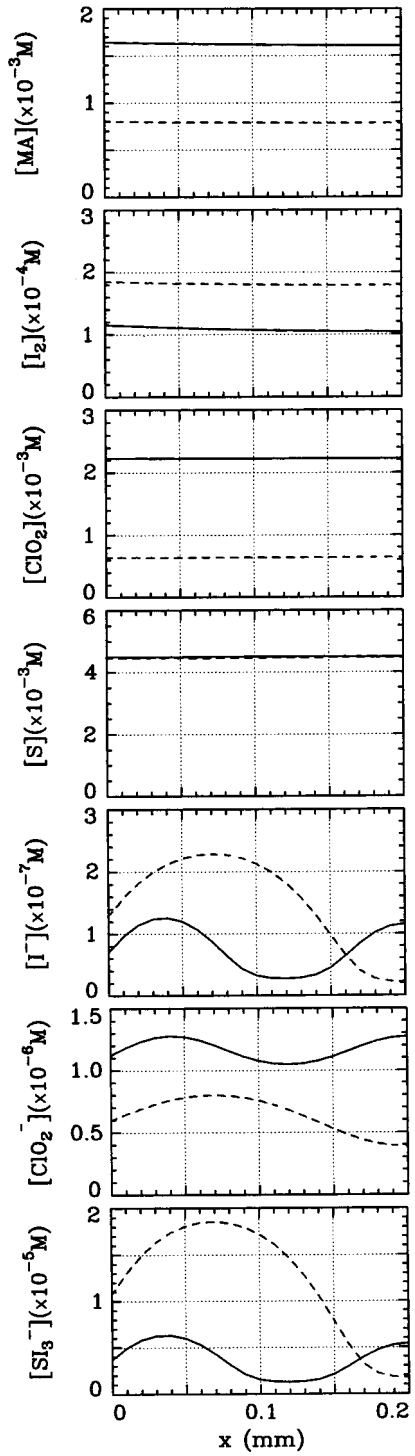

Figure 5. Numerical simulations of 1-D concentration profiles in the depth of the gel (LRE model). The CSTR is located at $x = 0$. Fixed parameters: $[S]_0 = 4.5 \times 10^{-3}$ M, $[I_2]_0 = 3 \times 10^{-4}$ M; —, $[MA]_0 = 2 \times 10^{-3}$ M, $[ClO_2]_0 = 2.3 \times 10^{-3}$ M; - - -, $[MA]_0 = 1 \times 10^{-3}$ M, $[ClO_2]_0 = 0.68 \times 10^{-3}$ M.

form, are reported in Figure 5. We can see that the concentrations of the input species [MA], [ClO_2], [I_2], and [S] can be considered as practically constant inside the gel. The same conclusions hold for temporal changes during the oscillating regime. Thus, we confirm both the validity of the approximations in the LE model and the absence of relevant concentration gradients of input species in the gel. Therefore we can use a "pool chemical" approximation and the simple and analytically tractable LE model (eqs 5) in place of the seven-variable LRE model to perform computations in higher dimensionalities.

To establish the phase diagrams that constitute the core of this paper, we assumed that the gel is thin enough to be considered as a two-dimensional system. Since the feedback effects on the CSTR of the reactions taking place in the gel are negligible, we used the concentrations that the input species would have inside an uncoupled CSTR to assign the actual parameter values a, d, and σ inside the gel. Remember that these concentrations are different from those in the flow: their asymptotic values were computed in the (uncoupled) CSTR almost instantaneously using the LRE model. Thereafter, the bifurcation lines can be determined by checking the parameter set against eqs 7 and 9. This procedure drastically reduces the amount of necessary computations. The general features of the 2-D patterns were determined by solving numerically eqs 5 on a square domain with periodic boundary conditions for a large set of input flows covering the experimental range. The integration was achieved with an implicit odd−even hopscotch method with step control,[49] adapted to the case of nonlinear reactions.[17] To compute the pool chemical parameters, one could have used the whole coupled system CSTR−gel rather than the values in the CSTR alone and taken the input species values at another point in the gel. Such computations, using the medium point of the 1-D reactor, provided identical results.[53] This supports the validity of the simple and efficient approach presented here.

The problems related to the possible tridimensional organization of the structure in the depth of the gel and the role of the boundary conditions onto the feeding face when the assumption of a bidimensional system is relaxed will be discussed in section 4.

3. Results

The CSTR dynamics and the patterns in the disk of gel were simultaneously monitored. However, to make easier the presentation of the results, we shall at first separate the description of the homogeneous dynamics of the CSTR from that of the spatial structures observed in the disk. Whereas the CSTR dynamics does not depend much on the gel dynamics, the reverse is not true and intricated spatial phenomena can occur in the disk of gel when the contents of the CSTR oscillate.

3.1. CSTR Dynamics. Beside temperature, flow rate, and sufuric acid concentration, the iodine feed concentration was kept constant during all the experiments.

Depending on the composition of the feed-stream, we can qualitatively distinguish three states, identified by their dynamics and the Pt-electrode potential value: a high-potential (>200 mV) steady state, an oscillatory state, and a low-potential (<200 mV) steady state. Different sections of the phase diagram of the CSTR were explored. Figure 6 exhibits the limits of the oscillatory state domain in the ($[MA]_0$, $[ClO_2]_0$) plane, in the absence of complexing agent. To emphasize the quenching effect of $[PVA]_0$ on the oscillatory dynamics, a planar section ($[MA]_0$, $[PVA]_0$]) for a relatively low value of [$ClO_2]_0$ is also provided (Figure 7). The region of oscillations is located between the two steady-state regions (high or low potential). However, at low $[ClO_2]_0$ (Figure 6) and at high $[PVA]_0$ (Figure 7) the domain of oscillation closes up and a smooth transition between the two qualitatively different steady states is obtained.

Phase diagrams computed with the seven-variable model including flow terms and our choise of adjustable kinetic parameters are also reported in Figures 6 and 7. The general features are in very good agreement with the experimental observations. The model predicts a subcritical Hopf bifurcation at low $[MA]_0$ and, at high $[MA]_0$, a saddle-loop bifurcation

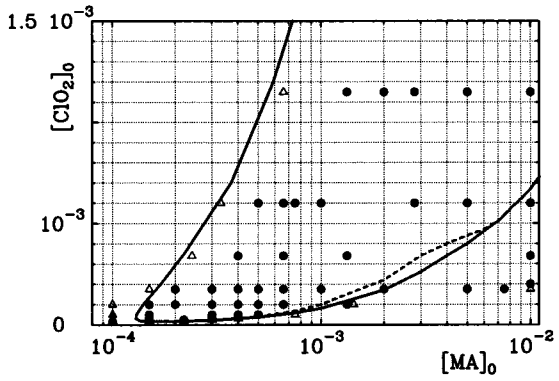

Figure 6. Planar section ($[MA]_0$, $[ClO_2]_0$) of the phase diagram of the CSTR at $[PVA]_0 = 0$. All other parameters are given in the text. Symbols correspond to experimental states (△, stationary; ●, oscillatory). Lines are the computed limits (—, limit of oscillations; - - -, limit of bistability between stationary state and oscillations).

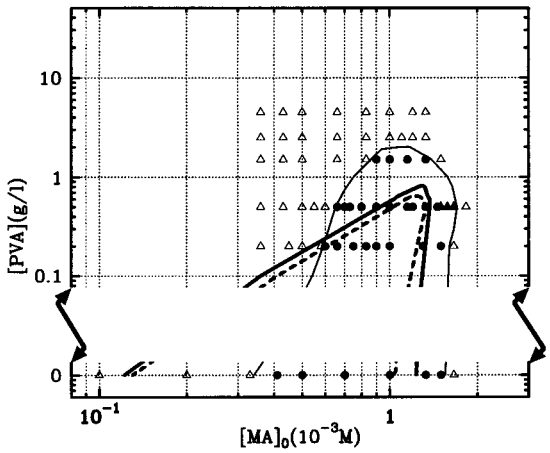

Figure 7. Planar section ($[MA]_0$, $[ClO_2]_0$) of the phase diagram of the CSTR at $[ClO_2]_0 = 1 \times 10^{-4}$ M. All other parameters are given in the text. Experimental observations: △, uniform stationary state; ▲, bistability between a stationary state and oscillations; ●, oscillatory state; —, experimental limit of oscillatory domain (estimated from these data); ━, computed limit of oscillations; ▪▪▪, computed limit of bistability between a stationary state and oscillations.

associated with a narrow region of bistability between a steady state and an oscillatory state (Figure 6). At low $[MA]_0$, no hysteresis is experimentally observed between the oscillatory state and the steady state. This was expected since, in the model, the width of the subcritical domain is of the order of the percent and thus would fall out of our experimental accuracy.

At the other limit of the oscillatory domain, in the absence of PVA (Figure 6), no hysteresis associated with a saddle-loop bifurcation is readily observed in experiments. However, the dynamics close to this limit of the phase diagram is consistent with what one would expect in the vicinity of such a bifurcation: oscillations exhibit large diverging periods and suddenly stop with finite amplitude. Nevertheless, a small region of hysteresis is experimentally observed at $[PVA]_0 = 0.5$ g/L (Figure 7).

Note that there is a significant difference between the predictions of the pool-chemical version of the LE model and the CSTR version: in the initial pool-chemical version, the domain of oscillations is unbounded on increasing $[MA]_0$ while, in the flow version, a steady state is recovered as in experiments. At a given value of $[ClO_2]_0$, there is a critical $[PVA]_0$ above which no homogeneous oscillatory state is observed. The model also nearly quantitatively fits this experimental fact (Figure 7).

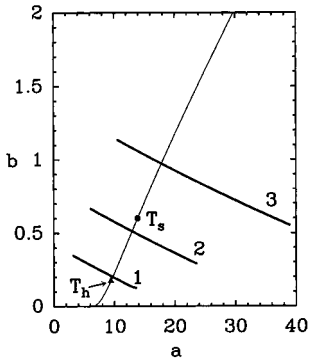

Figure 8. Parameter paths in the LE model when $[MA]_0$ is varied experimentally from 5×10^{-4} M up to the Hopf bifurcation (from left to right). Key: —, Turing bifurcation line (For points T_h and T_s, see Figure 2); ━, paths for $[ClO_2]_0 = 2.3 \times 10^{-3}$ M (path 1), $[ClO_2]_0 = 1.2 \times 10^{-3}$ M (path 2), $[ClO_2]_0 = 0.7 \times 10^{-3}$ M (path 3).

Note that this upper oscillatory state limit shifts to lower $[PVA]_0$ when $[ClO_2]_0$ is lowered.

To evaluate experimentally the contribution of flow terms to the oscillatory dynamics, the effect of interrupting the feed was examined. In general, the critical values of $[MA]_0$ after which oscillations immediately start are advanced by less than 10% when the flow is stopped. The oscillations then persist for at least 5 min. However, very often, the period increases by about 50% while the electropotential amplitude of oscillation decreases. This infers that in the region of constraint we explored, the "instantaneous" dynamics inside the CSTR does not dramatically depend on flow terms and that there is a fair chance that the homogeneous dynamics of the disk of gel should follow closely that of the CSTR. This agrees with the test numerical calculations previously presented in section 2.4 (Figure 5) that simulate the behavior in the thickness of the disk.

3.2. Phase Diagrams of Patterns in the Disk of Gel. The different regions of stationary and nonstationary spatial patterns breaking the boundary feed symmetry of the disk of gel were observed over a wide range of values of $[MA]_0$, $[ClO_2]_0$, and $[PVA]_0$. The results are gathered in different planar sections of the phase diagram. Before we discuss the contents of these sections, a few preleminary remarks are necessary.

The diagrams were established step by step using $[MA]_0$ as the bifurcation parameter. From each set of experimental input flow concentrations, one can compute the concentrations in the CSTR, from which are deduced, according to eq 6, the parameters (a, b) of the LE model used in the numerical simulations. To enlighten the comparison between the experimental and numerical results, we have represented (Figure 8) the paths in the (a, b) parameter space corresponding to the changes of $[MA]_0$ performed in experiments for three typical values of $[ClO_2]_0$ (high, medium, and low). The Turing bifurcation line is represented while the Hopf bifurcation lines are not since they depend on σ which continuously changes with the malonic acid concentration.

In the experiments, the light goes both across the gel and across a thin layer of reacting solution in the CSTR. Thus, when the contents of the CSTR oscillates, a nonstationary dynamics is always observed but the actual dynamics in the gel cannot be unambiguously determined. No comprehensive description of the intricated dynamics observed in these regions is attempted in this paper; more information can be found in ref 54. In Figure 9, we present the experimental and calculated sections of the phase diagram in the ($[MA]_0$, $[ClO_2]_0$) plane for two different fixed values of $[PVA]_0$. Three types of states are reported in these diagrams: the uniform steady states, the stationary Turing

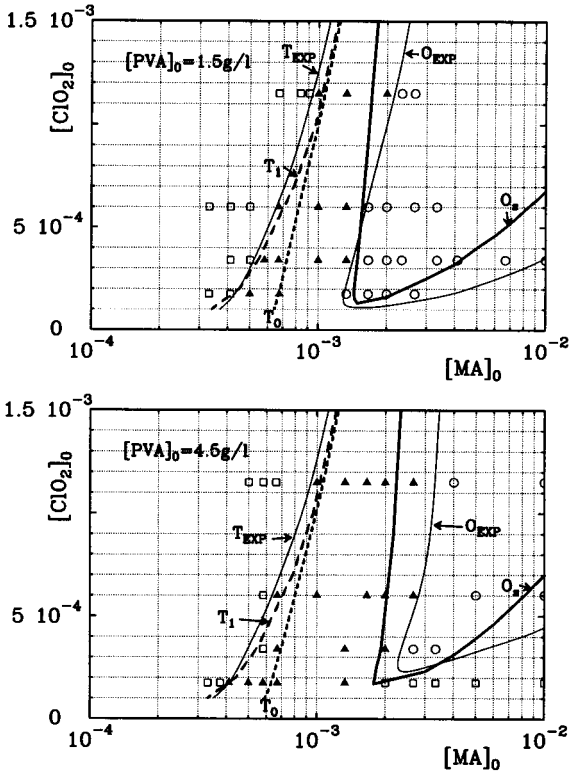

Figure 9. Plane section ($[MA]_0$, $[ClO_2]_0$) of the pattern phase diagram for two different values of [PVA]. Experimental observations: □, stationary uniform states; ▲, Turing patterns; ○, oscillatory states; —, limit of Turing (T_{EXP}) and oscillatory (O_{EXP}) domains (estimated from these data). Numerical simulations: ▪ ▪ ▪, Turing bifurcation (T_0); — —, limit of bistability between uniform and patterned states (T_1); —, limit of oscillatory domain (O_S).

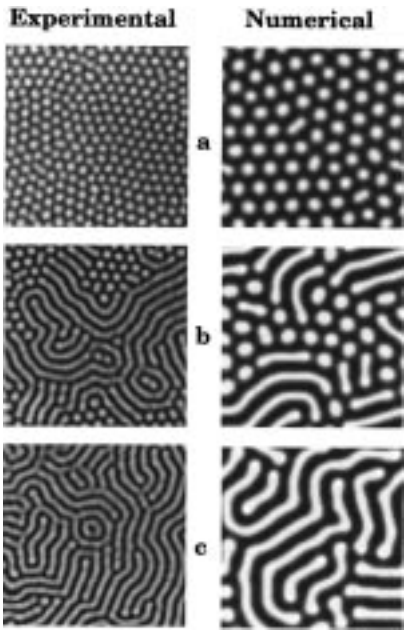

Figure 10. Sequence of patterns as a function of $[MA]_0$. Fixed parameters: $[PVA]_0 = 10$ g/L, $[ClO_2]_0 = 6 \times 10^{-4}$ M. Experimental data: (a) $[MA]_0 = 1.25 \times 10^{-3}$ M; (b) $[MA]_0 = 1.5 \times 10^{-3}$ M; (c) $[MA]_0 = 1.9 \times 10^{-3}$ M. Numerical data: (a) $[MA]_0 = 1.1 \times 10^{-3}$ M; (b) $[MA]_0 = 1.2 \times 10^{-3}$ M; (c) $[MA]_0 = 1.45 \times 10^{-3}$ M.

patterns which we strictly associate with non oscillatory states of the CSTR, and the nonstationary states including traveling waves and various oscillatory states which may or may not be associated with oscillations in the CSTR.

Considering the extreme simplicity of the LE model compared to the actual chemical kinetics, there is a striking agreement between computational and experimental results, at least when $[ClO_2]_0$ is not too low and $[PVA]_0$ not too high. In both cases, the Turing domain bracketed between a high $[SI_3^-]$ uniform steady state and an oscillatory state respectively at low and high $[MA]_0$ shifts to higher $[MA]_0$ as $[ClO_2]_0$ is increased. The computed Turing bifurcation line agrees almost quantitatively with the experimental line. The general features of the experimental and numerical Hopf lines also agree well, though the numerical limits are nearly systematically shifted forward with respect to the corresponding experimental lines.

There is also a very good agreement between computed and experimentally observed pattern planform distributions. In particular, the classical sequence of patterns when the distance to onset increases is well reproduced in both cases (Figure 10). If one starts from low $[MA]_0$ and increases this parameter, a transition occurs from the uniform dark state (high $[SI_3^-]$) to a stationary triangular array of clear spots, the H_π hexagon pattern of the model. When $[MA]_0$ is further increased, the spot patterns turns into a stationary stripe patterns. Although in experiments the domain of stripe patterns is less widespread than in the model, the general trends are followed. In both cases, the extent of the domain of stripes increases with $[ClO_2]_0$. The model even predicts that, at point T_h in Figure 3, reached for $[ClO_2]_0 = 2.5 \times 10^{-3}$ M, the H_π domain vanishes at onset and that, for larger values of $[ClO_2]_0$, a H_0 state should develop. The latter is not observed experimentally, but at such high values of $[ClO_2]_0$, the pattern amplitude becomes so small that any pattern would be difficult to detect experimentally. This problem is actually encountered when $[ClO_2]_0 > 1.4 \times 10^{-3}$ M; for these values, no patterned states were detected, even for large PVA concentrations.

There seems to be some discrepancy between the model calculations and the experiments at high $[PVA]_0$ and low $[ClO_2]_0$ below the oscillatory domain. In the experiments, when $[MA]_0$ increases, the Turing state is followed by a new uniform steady state, characterized by a lower value of complex $[SI_3^-]$ (clear color). No similar computed bound appears in Figure 9. As a matter of fact, when $[MA]_0$ increases, the computed stationary pattern becomes unstable and is replaced by an oscillatory state. Since the volume of the gel is small and in contact with the large volume of the CSTR which remains stationary, we suspect that, in the experiment, the gel does not oscillate because it is forced into a uniform steady state. This interpretation goes beyond our present 2-D approximation so that the computed limits are not really significant and have not been reported on the diagrams. More general considerations on the role of the coupling between the gel and the CSTR will be found in section 4.

At low $[ClO_2]_0$ values, the simulations predict that the domain where the uniform steady state and the stationary patterns are simultaneously stable (subcritical regime) tremendously increases since the experimental path crosses the Turing line above point T_S (see Figure 8). The limit of this domain is reported in Figure 9 (line T_1). At the same time, the patterns become very stiff and the dynamics slows down so that, at typical experimental times, they remain in a quasi-frozen state, retaining irregular planforms. Although no systematic bistability between a patterned state and a uniform state was found in the experiments, these tendencies were also observed. Coexistence of a pattern and a uniform state was actually found in a narrow region around point ($[MA]_0 = 7.8 \times 10^{-4}$ M, $[ClO_2]_0 = 2.5 \times 10^{-5}$ M) where localized patterns, a phenomenom linked to subcritical regimes,[55] were observed.[59] Moreover, when $[ClO_2]_0$

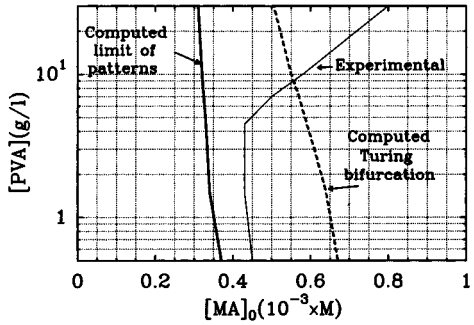

Figure 11. Dependence of the low $[MA]_0$ Turing limit on $[PVA]_0$ at $[ClO_2]_0 = 1 \times 10^{-4}$ M.

is decreased at constant $[MA]_0$, the experimental wavelength strongly increases and the patterns eventually disappear. In the simulations, the wavelength increases until it becomes larger than the system size itself. When this limit is reached, the patterns obviously vanish. Anyway, for the same reasons as previously mentioned, the 2-D approximation should break down in this limit where the pattern amplitude becomes excessively large.

According to ref 47, in the pool-chemical approximation, the addition of a *nonreactive* immobile complexing agent involved in a *fast reversible* process changes neither the steady-state solution nor the position of the Turing bifurcation line and the associated critical wavelength. Indeed, in the LE model, the Turing bifurcation point does not depend on σ. In flow reactors, there are additional sink terms of the form $k_e[SI_3^-]$ for the complex. They do not depend on an equilibrium with the complexing agent so that the steady-state value of the system should depend on the concentration of the complexing agent. Thus, the strict invariance of the Turing bifurcation on the concentration of such a complexing agent should drop in our CSTR/gel system.

However, the dependence of the Turing bifurcation line with $[PVA]_0$ is usually minor, both in calculations and in experiments, as shown in Figure 9 by comparing the low $[MA]_0$ limit of the Turing domain at different values of $[PVA]_0$. To test the extent of such an invariance, a systematic study of the onset of Turing patterns was performed as a function of $[PVA]_0$ at $[ClO_2]_0 = 1 \times 10^{-4}$ M. This relatively low value was chosen in order not to be hindered by losses of contrast of patterns when $[PVA]_0$ is decreased. Figure 11 gathers the experimental and computed results of this study. For this low $[ClO_2]_0$ value the model predicts a large subcritical domain of Turing patterns. The computed Turing bifurcation line and the limit of this subcritical domain are reported in Figure 11. The two lines evolve nearly parallelly as a function of PVA and bracket the experimentally observed transition line, at low $[PVA]_0$. As already mentioned, hysteresis is not observed within our experimental concentration step changes, i.e., 10% around the drawn transition line.

Calculations show that the presence of flow terms slightly shifts the Turing bifurcation to lower values of $[MA]_0$ as the PVA concentration is increased. However, this shift becomes significant only at low $[ClO_2]_0$ values. This is consistent with the fact that the lower is the $[ClO_2]_0$ value the larger is the difference between the flow value and the concentration of ClO_2 in the reactor. In experiments, a similar deviation is first observed at low $[PVA]_0$, but when $[PVA]_0 > 4.5$ g/L, an additional stronger deviation develops in the opposite direction. This shift depends on the thickness of the disk of gel: for a thickness of 0.5 mm, the position of the Turing transition line is basically unchanged at low [PVA] while the shift to high $[MA]_0$ vanishes even for $[PVA]_0 = 10$ g/L. This shift cannot be accounted for by the presence of flow terms. One could evoke the participation of PVA in reactions other than complexation or the fact that the strong increase in the viscosity of the solution might affect some fast steps in the reaction.

TABLE 1: Pattern Wavelength at $[PVA]_0 = 4.5$ g/L

$10^4[ClO_2]_0$ (M)	exptl λ (mm)	numerical λ (mm)	$10^4[ClO_2]_0$ (M)	exptl λ (mm)	numerical λ (mm)
1	0.41 ± 0.02	0.38	3.5	0.28 ± 0.02	0.24
1.75	0.33 ± 0.02	0.33			

A comparison of the wavelength dependence on $[MA]_0$, $[ClO_2]_0$, and $[PVA]_0$ can be established between the experiments and our model system. In both cases, the wavelength of the Turing patterns depends little or not on malonic acid. This common property allows us to compare the wavelength λ at experimental and computed points which only differ in malonic acid, to counterbalance the slight shift between the observed and calculated phase diagrams. Table 1 gathers a sample of experimental and computed wavelengths as a function of $[ClO_2]_0$. The wavelength of the pattern is very sensitive to $[ClO_2]$. The agreement between the observed and computed relative changes as a function of $[ClO_2]_0$ is excellent. The experimental wavelength slightly depends on $[PVA]_0$ when this concentration is high, whereas it is independent in the calculations. The calculated independence of λ on [PVA] is akin with the predicted invariance in pool-chemical systems.[47] The experimental increase of wavelength with [PVA] suggests that the relative decrease in the chemical time is greater than that of the diffusion time of iodide. This could result from a difference between the effective concentration of complexing sites per unit weight of polymer in the free solution of the CSTR and in the gel matrix.

Let us mention incidentally experimental observations relative to a narrow domain of parameter along the limit between stationary and nonstationary patterns (Figure 9). Inside the gel, oscillatory behaviors can anticipate the Hopf bifurcation in the CSTR. In this marginal domain, spatio−temporal patterns reminiscent of Turing−Hopf mixed modes,[56] similar to those already reported in two-side-fed reactors,[57] can be observed. Yet, here the spatio−temporal behavior is not complicated by the parameter ramps inseparable of two-side-fed gel reactors.[58]

4. Discussion and Conclusion

The main conclusion of this systematic study is that, despite its formal simplicity, the two variable Lengyel−Epstein model accounts quasi quantitatively for the main features of Turing patterns observed in the (ClO_2−I_2−MA) reaction provided that the *ad-hoc* constant α of the model is properly chosen. Computations are made easy and can be readily connected to the analytically calculable properties of the model since the one-side-fed thin gel reactor provides a good approximation of the pool-chemical hypothesis. This relies on the slow concentration variations of the input species and on the characteristic diffusion time in the depth of the gel. The only noticeable discrepancies appear in marginal domains and when $[ClO_2]_0$ is very low or $[PVA]_0$ is high. They essentially point out the limits of the approximations and reveal some previously overlooked problems directly associated with the actual status of boundary conditions and dimensionality.

As a matter of fact, a careful theoretical analysis reveals some serious difficulties that need additional explanations. Up to now, we have assumed that the patterns can be considered as two-dimensional, i.e. the spontaneously selected structures are made of short isoconcentration "walls" (stripes) or "columns" (spots)

orthogonal to the faces. From this point of view, the thinner the gel, the better the two-dimensional approximation should be. A thickness equal to a wavelength or less would seem appropriate but a new problem then arises. The feed-face of the disk in contact with the CSTR is permanently kept homogeneous, defining a uniform Dirichlet boundary condition, and no pattern can form in the vicinity of this face. When the system is thin, the influence of this boundary condition would extend over the whole gel and all transverse instabilities (i.e. parallel to the feed-surface) should be hindered. To explore the consequences of the nature of boundary conditions on pattern selection, we have performed a few 3-D computations with the LE model.[53,60] In the following, we only report the conclusions. When the system is forced with a Dirichlet boundary condition onto the feed-face and the thickness is $l \leq \lambda/4$, the transverse instability is always inhibited so that a uniform light absorption would be obtained through the gel and no pattern would be detected. Moreover, for slightly thicker systems, nonregular patterns form. On the contrary, in pool-chemical conditions with no flux boundaries on both sides, the system behaves as two-dimensional for almost all thicknesses in the range $0 < l < \lambda$, developing the correct planforms, but such boundary conditions obviously exclude any realistic feed process. To understand the successful 2-D interpretation of the experiments of section 3, we have to reconsider the nature of the boundary conditions. As a matter of fact, the contact between the gel and the CSTR contents is achieved through a membrane (section 2.1). Moreover a boundary layer in the turbulent fluid of the CSTR very likely forms along the membrane, decreasing the efficiency of exchanges and mixing in the vicinity of the feed-surface. The interface "membrane + boundary layer", hereafter referred for simplicity as the "membrane", introduces some partial decoupling between the bulk of the CSTR and the gel. As a first approach, we can describe the effect of this membrane in a phenomenological way by using a mixed boundary condition at the feed-interface. With finite difference equations this is conveniently obtained using the following formula for the diffusion term in the *z*-direction, orthogonal to the faces:

$$\frac{\partial C_0}{\partial t} = \frac{2D}{(\Delta z)^2}\left[(C_1 - C_0) + \frac{\Delta z}{e_m}(C_e - C_0)\right] \qquad (11)$$

Here C_e is the concentration in the CSTR, C_0 the concentration at the grid point of the gel at the interface, C_1 the concentration at the first point inside the gel, and Δz the spatial stepsize. The effects of the membrane are contained in the phenomenological parameter e_m, which has the dimension of a length and can be considered as a kind of effective thickness (to be distinguished from the physical thickness!) of the membrane that holds for all phenomena which take place within it. When $e_m \rightarrow 0$ (no membrane), Dirichlet boundary conditions are recovered, whereas when $e_m \rightarrow \infty$ (complete decoupling), no flux boundary conditions are recovered. We have found that values of e_m in the range 0.1−0.2 mm (the same order of magnitude that the physical thickness) introduce an appropriate decoupling which restores, in most cases, the 2-D behavior.[53] This can be understood from the 1-D simulations reported in Figure 12, analogue to those of Figure 5, but where the effect of the membrane for different values of parameter e_m are compared to the case $e_m = 0$. Despite the partial decoupling introduced at the interface, the changes induced by the membrane for the concentrations at this interface are rather small (they are the largest for I_2) and the pool-chemical approximation inside the gel is preserved. On the contrary, the profiles of the intermediate species are strongly modified, gaining a quasi-horizontal tangent

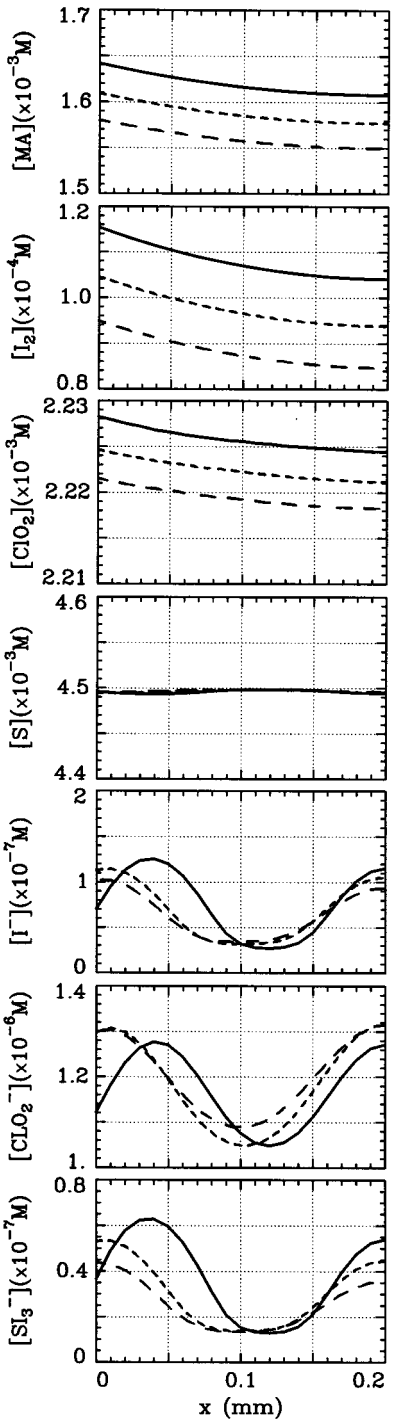

Figure 12. Numerical simulations of 1-D concentration profiles in the thickness of the gel (LRE model) with and without membrane. The interface is located at $x = 0$. Key: $[S]_0 = 4.5 \times 10^{-3}$ M, $[I_2]_0 = 3 \times 10^{-4}$ M, $[MA]_0 = 2 \times 10^{-3}$ M, $[ClO_2]_0 = 2.3 \times 10^{-3}$ M; —, $e_m = 0$ (no membrane, full coupling); - - -, $e_m = 0.1$ mm; — —, $e_m = 0.2$ mm.

at the interface, the signature of no flux boundary conditions which are required to restore the validity of the 2-D approximation.

Thus, there is almost perfect coupling for the species that correspond to the input parameters and almost perfect decoupling for those which are intimately involved in the pattern formation dynamics. The minor changes in input species concentrations might only induce a small shift in the onset of Turing patterns, but the general trends discussed in section 3 should be preserved. Note that this description is different from the so-called CFUR approximation,[61] since, despite the phe-

nomenological description of the membrane, the feed remains located *at the boundary* and the system is treated as tridimensional but the *selected structure* is bididimensional. To check the validity of this interpretation, the coupling between CSTR and the gel was changed in a few test experiments. A stronger coupling was obtained by withdrawing the Anotec membrane from the interface. In this case, the onset of Turing patterns is delayed and the extent of their domain is reduced by about a factor of 3, while, on doubling the membrane at the interface, only a very slight advance of the onset of patterns by 5% is observed. Thus, we confirm the major role played by the coupling strength at the interface on the formation of Turing patterns. More generally, the genuine nature of the boundary conditions should be taken into account, especially in the case of one-side-fed reactors where reactions start before chemicals diffuse into the gel.

Until now, this important boundary problem has been nearly systematically overlooked in the chemical patterns literature, and we think that a number of experimental observations cannot be understood without a clear perception of the role played by the interfaces.[62]

Acknowledgment. This work has been partly supported by the NATO program COP910520. B.R. received a fellowship in the frame of the French−Hungarian cooperation program. Our interest for these topics was stimulated by numerous discussions with P. Borckmans, G. Dewel, I. R. Epstein, I. Lengyel, and A. De Wit.

References and Notes

(1) Turing, A. M. *Philos. Trans. R. Soc. London* **1952**, *B327*, 37.
(2) Meinhardt, H. *Models of Biological Patterns Formation*; Academic Press: New York, 1982. Meinhardt, H. *Prog. Rep. Phys.* **1992**, *55*, 797−849.
(3) Murray, J. D. *Mathematical Biology*; Springer-Verlag: New York, 1989.
(4) Harrison, L. G. *J. Theor. Biol.* **1987**, *185*, 369. Harrison, L. G. *Kinetic Theory of Living Pattern*; Cambridge University Press: Cambridge, U.K., 1992.
(5) Koch, A. J.; Meinhardt, H. *Rev. Mod. Phys.* **1994**, *66*, 1481−1507.
(6) Castets, V.; Dulos, E.; Boissonade, J.; De Kepper, P. *Phys. Rev. Lett.* **1990**, *64*, 2953.
(7) De Kepper, P.; Epstein, I. R.; Kustin, K.; Orbán, M. *J. Phys. Chem.* **1982**, *86*, 170.
(8) De Kepper, P.; Boissonade, J.; Epstein, I. R. *J. Phys. Chem.* **1990**, *94*, 6525.
(9) De Kepper, P.; Castets, V.; Dulos, E.; Boissonade, J. *Physica D* **1991**, *49*, 161.
(10) Ouyang, Q.; Swinney, H. L. *Nature* **1991**, *352*, 610.
(11) Ouyang, Q.; Swinney, H. L. *Chaos* **1991**, *1*, 411.
(12) Kapral, R.; Showalter, K. *Chemical Patterns and Waves*; Klüwer: Amsterdam, 1995.
(13) Prigogine, I.; Lefever, R. *J. Chem. Phys.* **1968**, *48*, 21695.
(14) Haken, H.; Olbrich, H. *J. Math. Biol.* **1978**, *317*, 137.
(15) Walgraef, D.; Dewel, G.; Borckmans, P. *Adv. Chem. Phys.* **1982**, *49*, 311.
(16) Dufiet, V.; Boissonade, J. *J. Chem. Phys.* **1991**, *96*, 664−673.
(17) Dufiet, V.; Boissonade, J. *Physica* **1992**, *A188*, 158−171.
(18) Verdasca, J.; De Wit, A.; Dewel, G.; Borckmans, P. *Phys. Lett.* **1992**, *A168*, 194.
(19) Borckmans, P.; De Wit, A.; Dewel, G. *Physica* **1992**, *A188*, 137.
(20) Hunding, A. *Physica* **1992**, *A188*, 172.
(21) Lengyel, I.; Epstein, I. R. *Science* **1990**, *251*, 650.
(22) Lengyel, I.; Epstein, I. R. *Proc. Natl. Acad. Sci. U.S.A.* **1992**, *89*, 3977.
(23) Lengyel, I.; Kádár, S.; Epstein, I. R. *Phys. Rev. Lett.* **1992**, *69*, 2729.
(24) Epstein, I. R.; Lengyel, I.; Kádár, S.; Kagan, M.; Yokoyama, M. *Physica* **1992**, *A188*, 26.
(25) Lengyel, I.; Epstein, I. R. *Acc. Chem. Res.* **1993**, *26*, 235.
(26) Epstein, I. R.; Lengyel, I. *Physica* **1995**, *D84*, 1.
(27) Epstein, I. R.; Lengyel, I. In ref 12, p 297.
(28) Lengyel, Rábai, I.; Epstein, I. R. *J. Am. Chem. Soc.* **1990**, *112*, 4606.
(29) Lengyel, Rábai, I.; Epstein, I. R. *J. Am. Chem. Soc.* **1990**, *112*, 9104.
(30) Kádár, S.; Lengyel, I.; Epstein, I. R. *J. Phys. Chem.* **1995**, *99*, 4054.
(31) Agladze, K.; Dulos, E.; De Kepper, P. *J. Phys. Chem.* **1992**, *96*, 2400.
(32) Noszticzius, Z.; Ouyang, Q.; McCormick, W. D.; Swinney, H. *J. Phys. Chem.* **1992**, *96*, 6302.
(33) Boissonade, J.; Castets, V.; Dulos, E.; De Kepper, P. *Int. Ser. Numer. Math.* **1991**, *97*, 67.
(34) Ouyang, Q.; Noszticzius, Z.; Swinney, H. L. *J. Phys. Chem*. **1992**, *96*, 6773.
(35) Dulos, E.; Davies, P.; Rudovics, B.; De Kepper, P. *Physica D* **1996**, *98*, 56.
(36) Dufiet, V.; Boissonade, J. *Phys. Rev. E* **1996**, *53*, 4883.
(37) Rovinsky, A.; Menzinger, M. *Phys. Rev. A* **1992**, *46*, 6315.
(38) By "phase", we mean a dynamical state which characterizes unambiguously the asymptotic regime.
(39) Nagypal, I. Private communication.
(40) Kern, D. M.; Kim, C. H. *J. Am. Chem. Soc.* **1992**, *87*, 5309.
(41) Lengyel, I.; Li, J.; Kustin, K.; Epstein, I. R. *J. Am. Chem. Soc.* **1996**, *118*, 3708.
(42) De Meeus, J.; Sigalla, J. *J. Chim. Phys.-Chim. Biol.* **1966**, *63*, 453.
(43) Leopold, K. R.; Haim, A. *Int. J. Chem. Kinet.* **1977**, *9*, 83.
(44) Lengyel, I.; Epstein, I. R. *J. Phys. Chem.* **1992**, *96*, 7032.
(45) Boissonade, J.; De Kepper, P. *J. Chem. Phys.* **1987**, *87*, 210.
(46) Borckmans, P.; Dewel, G.; De Wit, A.; Walgraef, D. In ref 12, p 323.
(47) Pearson, J. E.; Bruno, W. J. *Chaos* **1992**, *2*, 513.
(48) Kaps, P.; Rentrop, P. *Numer. Math.* **1979**, *33*, 55.
(49) Gourlay, A. R. *J. Inst. Math. Its Appl.* **1970**, *6*, 375. Gourlay, A. R.; McGuire, G. R. *J. Inst. Math. Its Appl.* **1971**, *7*, 216.
(50) Manneville, P. *Dissipative structures and weak turbulence*; Academic Press: New York, 1990.
(51) Malomed, B. A.; Tribel'skii, M. I. *Sov. Phys. JETP* **1987**, *65*, 305.
(52) Ciliberto, S.; Coullet, P.; Lega, J.; Pampaloni, E.; Perez-Garcia, C. *Phys. Rev. Lett.* **1990**, *65*, 2370.
(53) Barillot, E. Ph.D. Thesis, Bordeaux, 1996.
(54) Rudovics, B. Ph.D. Thesis, Bordeaux, 1995.
(55) Jensen, O.; Pannbacker, V. O.; Dewel, G.; Borckmans, P. *Phys. Lett.* **1993**, *A179*, 91.
(56) De Wit, A.; Lima, D.; Dewel, G.; Borckmans, P. *Phys. Rev. E* **1996**, *54*, 261.
(57) De Kepper, P.; Perraud, J.-J.; Rudovics, B.; Dulos, E. *Int. J. Bif. Chaos* **1994**, *4*, 1215.
(58) Rudovics, B.; Dulos, E.; De Kepper, P. *Phys. Scr.* **1996**, *T67*, 43.
(59) Davies, P.; Blanchedeau, P.; Dulos, E.; De Kepper, P. *J. Phys. Chem.* **1998**, *102*, 8236.
(60) Boissonade, J. Unpublished results.
(61) Vastano, J. A.; Pearson, J. E.; Horsthemke, W.; Swinney, H. L. *J. Chem. Phys.* **1988**, *88*, 6175.
(62) Blanchedeau, P.; Boissonade, J. *Phys. Rev. Lett.* **1998**, *81*, 5007.